Thermodynamic modelling of synthetic communities predicts minimum free energy requirements for sulfate reduction and methanogenesis.

Hadrien Delattre[1,*,^], Jing Chen[1,*,#], Matthew Wade[2], Orkun S Soyer [1,^]

[*]These authors contributed equally to this work. [^]Corresponding authors.
[1]School of Life Sciences, University of Warwick, UK.
[2] School of Engineering, Newcastle University, Newcastle-upon-Tyne NE1 7RU UK.
[#]Current address: School of Chemical Engineering, Sichuan University, Chengdu, Sichuan Province, China 610065

ABSTRACT

Microbial communities are complex dynamical systems harbouring many species interacting together to implement higher-level functions. Among these higher-level functions, conversion of organic matter into simpler building blocks by microbial communities underpins biogeochemical cycles and animal and plant nutrition, and is exploited in biotechnology. A prerequisite to predicting the dynamics and stability of community-mediated metabolic conversions, is the development and calibration of appropriate mathematical models. Here, we present a generic, extendable thermodynamic model for community dynamics accounting explicitly for metabolic activities of composing microbes, system pH, and chemical exchanges. We calibrate a key parameter of this thermodynamic model, the minimum energy requirement associated with growth-supporting metabolic pathways, using experimental population dynamics data from synthetic communities composed of a sulfate reducer and two methanogens. Our findings show that accounting for thermodynamics is necessary in capturing experimental population dynamics of these synthetic communities that feature relevant species utilising low-energy growth pathways. Furthermore, they provide the first estimates for minimum energy requirements of methanogenesis and elaborates on previous estimates of lactate fermentation by sulfate reducers. The open-source nature of the developed model and demonstration of its use for estimating a key thermodynamic parameter should facilitate further thermodynamic modelling of microbial communities.

INTRODUCTION

Microbial communities are found in diverse habitats including the oceans, soil, animal guts, and plant roots. The interconnected metabolic activities in these microbial communities underpin the biogeochemical cycles that feed into the Earth's ecosystem [1] and the nutrient cycles that support the growth of animals and plants [2, 3]. The same community level metabolic activities, and in particular anaerobic digestion (AD), are also exploited in biotechnology for water treatment and bioenergy production from organic waste [4]. Thus, the ability to capture microbial growth rates and metabolic activities within microbial communities is identified as an important prerequisite for the predictive modelling of planetary ecosystem dynamics, animal and plant health, and biotechnological waste valorisation [4].

Modelling microbial community dynamics is a significant challenge due to the complexity of these systems. Typical communities, for example those found in human gut or AD reactors, are composed of 100s to 1000s of distinct microbial species [5, 6]. The metabolic activities, and hence the growth, of these different species are interlinked to each other through metabolic interactions that resemble ecological ones [7]. This resemblance has motivated the adaptation of simplified ecological models (e.g. Lotka-Volterra models) to the modelling of microbial communities [8]. While these models allow drawing generalised hypotheses about the role of

different types of interactions on microbial community stability [9], they do not capture metabolite dynamics, which are shown to be essential for predicting population dynamics [10].

Microbial growth and metabolite dynamics are historically captured by empirical models such as the Monod growth function [11, 12]. These growth functions have been used to capture dynamics of microbial communities, most notably to construct relatively large-scale models describing AD communities, as used in wastewater treatment engineering [13]. These models reduce system complexity by considering functional groups (so-called 'guilds'), rather than individual species, thereby capturing key metabolic processes and interactions such as polymer degradation, sulfate reduction, and methanogenesis [14, 15]. The guild-based approach makes it possible to calibrate and test these models against the key metabolites measured in AD reactors, bringing us closer to predicting performance and stability of communities in biotechnological applications. Towards achieving this goal, however, a key limitation has been the inadequacy of Monod-type models to capture microbial metabolic conversions that are at a low energy level, and thus operating close to thermodynamic equilibrium [16, 17]. Such 'thermodynamic inhibition' of microbial growth and metabolism is highly relevant to AD, as well as soil, sediment, and gut communities, where there is commonly a depletion of strong electron acceptors and a shift of metabolism from high energy respiratory pathways to low energy fermentative pathways [18].

To capture thermodynamic inhibition effects, a simple thermodynamic model has been proposed that adjusts a Monod-type growth function with a thermodynamic factor based on the free energy of the growth-supporting metabolic conversion [16, 17, 19, 20]. This approach is further elaborated upon by considering the fact that part of the free energy from a given metabolic conversion must be invested into cellular maintenance and as a metabolic driving force, thus defining a minimal energy threshold for a growth-supporting pathway [21]. Incorporating such a thermodynamic model has allowed studying the basis of observed diversity in microbial communities [22] and making qualitative predictions on population dynamics in microbial communities [23]. A fully quantitative prediction of population and metabolite dynamics, however, requires that these models implement specific, calibrated kinetic and thermodynamic parameters for each of the accounted microbial species and their metabolic conversions.

Kinetic parameters of microbial growth have been collected over decades of research using monocultures grown under defined conditions. In particular, maximal growth rate (v_{max}), substrate affinity coefficient (K_s), and biomass yield from substrate ($Y_{s/x}$) have been experimentally estimated for individual species that represent common functional groups seen in microbial communities. For some of these kinetic parameters, in particular biomass yield and substrate uptake rate, calibrated methods have been derived that can predict parameters from existing data and first principles approximations [24–26]. The key thermodynamic parameter, namely the minimum energy threshold of different metabolic conversions, however, remains mostly unavailable. Moreover, there has not been any focussed exploration of what kind of experimental measurements can provide sufficiently robust estimations for this parameter. This situation limits the applicability of thermodynamic community models, which are required to fully capture the growth of many functionally relevant species.

Here, we aim to address this gap and develop a generic, readily extendable thermodynamic community model and use it to estimate the minimal free energy parameters from experimental time-series data. The model implements the multiple and distinct growth-supporting metabolic conversions possible in each organism and accounts for their possible thermodynamic

limitations. It also accounts for metabolite phase exchanges and system pH. We calibrate the model using experimental data from synthetic communities composed of microbial species that represent key functional groups in AD systems; *Desulfovibrio vulgaris* (*Dv*), a sulfate reducer, *Methanococcus maripaludis* (*Mm*), a hydrogenotrophic methanogen, and *Methanosarcina barkeri* (*Mb*), a methanogen capable of acetoclastic methanogenesis. Using daily metabolite measurement from mono-, co-, and tri-cultures over a 21-day experiment, we show that the resulting model provides a superior fit to data, compared to a non-thermodynamic model, and that some of the thermodynamic parameters of the model can be calibrated using time-series data. These results show that thermodynamic models are appropriate and are needed to accurately capture metabolite dynamics in microbial communities, but that their full calibration requires a greater breadth of experimental data.

MATERIALS AND METHODS

Overall model description and availability. The model presented here aims to capture the population and metabolic dynamics within a microbial monoculture or a multi-species community. The model accounts for a set of growth-supporting metabolic pathways that involve either specific metabolites or cellular biomass (Figure 1). The chemical speciation of metabolites, as well as their exchange between gas and liquid phases is accounted for. The medium pH is also simulated based on the set of acid-base reactions that are included. The model is developed in a generic and user-accessible manner, so that growth-supporting reactions, species involved, gas/liquid exchange reactions, and acid-base reactions can be supplied by the user without any pre-requisite programming skills, and the source-code is extendable by advanced users. The entire model is encoded in an object-oriented software using Python 3.4 and the source-code and simulation manual are provided via authors' research website at https://github.com/OSS-Lab/micodymora.

Growth supporting metabolic pathways. For the presented model, several growth-supporting (i.e. catabolic) and biomass forming (i.e. anabolic) metabolic pathways are considered to be encoded by *Dv*, *Mm* and *Mb* populations, as illustrated in Figure 1A and listed in Table 1. The anabolic (biomass producing) reactions of *Dv*, *Mm* and *Mb* populations are considered to utilise lactate, carbon dioxide, and acetate respectively as carbon source. In each of these reactions, biomass is represented as a generic molecule (with chemical formula $C_1H_{1.8}O_{0.5}N_{0.2}$), having an associated Gibbs free energy of formation of -67 kJ/mol [27]. Table 1 lists all growth-supporting catabolic reactions modelled in this work, along with their associated Gibbs free energy ($\Delta G^{0\prime}$) calculated at a pH of 7.0 and a temperature of 310.15 K with reagents other than protons in their standard state.

Modelling population and metabolite dynamics. To model population dynamics, we consider the *Dv*, *Mm* and *Mb* populations as implementing catabolic pathways available for each species. The overall dynamics of each population are governed by a differential equation that accounts for all of its catabolic pathways rates, as well as its anabolic biomass production. It is assumed that for a given population, the anabolic reaction has the same formula for each of its catabolic pathways (see Table 1). To represent the moles of biomass formation per moles of catabolite consumed, the stoichiometry of each anabolic reaction is multiplied by a dynamic yield coefficient (Y, in mol_X/mol_S where X stands for biomass and S for the substrate by which the catabolic pathway's formula is normalized). This yield coefficient is computed dynamically from the energetics of catabolic and anabolic reactions, as well as the dissipated energy during biomass formation;

$$Y_{i,j} = \frac{\Delta G^i_{cat,j}}{\Delta G^i_{diss,j} - \Delta G^i_{an}} \qquad \text{Eq. 1}$$

where the indices *i* and *j* range over a given species (e.g. *Dv*) and catabolic pathway (e.g. lactate fermentation) respectively. The $\Delta G^i_{cat,j}$ is the Gibbs free energy (in kJ/mol$_S$), of the associated catabolic pathway *j* in a given species *i*, while $\Delta G^i_{diss,j}$ is the dissipated energy in anabolism for the same pathway. ΔG^i_{an} is the Gibbs free energy of the anabolic reaction respectively (both in kJ/mol$_X$) for species *i*. The Gibbs free energy of the catabolic and anabolic reactions are calculated dynamically during model simulation from the chemical species concentrations. The dissipated energy is that which is harvested by the population through its catabolism and which is not chemically stored as biomass. It encompasses a wide diversity of processes including heat and entropy emission and cellular maintenance. Its value is estimated based on experimentally measured dissipated energy for different microbial species [28] (see Table 1).

The specific rate ($r_{i,j}$ in mol$_S$/(mol$_X$·hour)) of a catabolic pathway *j* for a given species *i* is given by;

$$r_{i,j} = \left(\nu^i_{\max,j} \prod_k \frac{\left[S^j_k \right]}{K_{S^j_k} + \left[S^j_k \right]} \right) \cdot \left(1 - e^{\frac{\min\left(0, \Delta G^i_{cat,j} - \Delta G^i_{\min,j}\right)}{R \cdot T}} \right) \qquad \text{Eq. 2}$$

where $\nu^i_{\max,j}$ is the maximum catabolic turnover rate, expressed in mol$_S$/(mol$_X$·hour) and specific to the pathway *j* and the population *i*, $\left[S^j_k \right]$ is the concentration of the k^{th} limiting substrate of the pathway *j*, $K_{S^j_k}$ is the half-saturation coefficient for that substrate, $\Delta G^i_{cat,j}$ is the Gibbs free energy of the catabolic reaction *j* for species *i*, and $\Delta G^i_{\min,j}$ is the minimum energy threshold for that catabolic reaction. This last term ($\Delta G^i_{\min,j}$) captures how energy-storing reactions coupled to the catabolic reaction (e.g. conserved moieties regeneration, proton extrusion, etc.) affects its rate. *R* (in J/(mol·K)) and *T* (in K) denote the gas constant and system temperature respectively. Note that in the main text, we refer to the first and second terms of Equation 2 as kinetic (F_D) and thermodynamic (F_T) factors, similar to previous presentations in the literature [29]. The kinetic coefficients $\nu^i_{\max,j}$ and $K_{S^j_k}$ are compiled from the literature and are listed in Supplementary Table S1.

Using the rate of the catabolic pathway and biomass yield of the anabolic pathway, we can write a differential equation describing the dynamics of the concentration of any chemical *A* according to the catalytic activity of each population;

$$\frac{d\left[A\right]}{dt} = \sum_i \left(\left[X_i \right] \cdot \sum_j \left(r_{i,j} \cdot \left(\gamma_{i,A} \cdot Y_{i,j} + \vartheta_{i,j,A} \right) \right) \right) \qquad \text{Eq. 3}$$

where $[X_i]$ represent the biomass concentration of the i'th population, $\gamma_{i,A}$ is the stoichiometric coefficient for chemical A in the anabolic reaction of the i'th population, and $\vartheta_{i,j,A}$ is the stoichiometric coefficient for chemical A in the j'th catabolic pathway of the i'th population.

The dynamics of the biomass associated to a population i obeys essentially the same equation as for the concentration of chemical (Equation 3), however, $\vartheta_{i,j,X}$ is always zero because biomass is not produced or consumed by catabolism and $\gamma_{i,X}$ is always one because the anabolic formula is normalized to the mole of biomass. Additionally, we account for the loss of biomass through death using a linear decay coefficient k_d (1/hour), resulting in the following differential equation for biomass;

$$\frac{d[X_i]}{dt} = [X_i] \cdot \left(\sum_j \left(r_{i,j} \cdot Y_{i,j} \right) - k_d \right) \qquad \text{Eq. 4}$$

We assume in the current model that k_d (=8.33e-4 1/h) is the same for all species. This value is based on the experimental estimates made on *Desulfovibrio vulgaris* monocultures [30].

Modelling of gas/liquid transfer. Some chemicals exist in both the gas and liquid phases. Any of such chemical species, A, is accounted for as two separate chemical species *A(aq)* and *A(g)* respectively. The concentrations of each species are accounted for by moles per liter of their respective phase volume. The transfer dynamics occurring between the two forms is captured through a set of differential equations given by;

$$\frac{d[A(aq)]}{dt} = k_L a \cdot \frac{V_{aq}}{V_g} \cdot \left([A(aq)] - [A(g)] \cdot H_{310.15} \right)$$
$$\frac{d[A(g)]}{dt} = -k_L a \cdot \left([A(aq)] - [A(g)] \cdot H_{310.15} \right) \qquad \text{Eq. 5 \& 6}$$

where k_La is the mass transfer coefficient of the chemical (in 1/hour) [31], $H_{310.15}$ is the Henry constant of the chemical at 310.15K (and expressed in mol/(m^3·Pa)), V_{aq} is the volume of the liquid phase and V_g is the volume of the gas phase (both in liters). Henry constants were obtained from the literature [32], and adjusted for a temperature of 310.15 K using the relation between Henry's constant and the solution enthalpy (ΔH_{sol}) as follows; $H_{310.15} = H_{298.15} \cdot \exp\left(\frac{\Delta H_{sol}}{R} \cdot \left(\frac{1}{310.15} - \frac{1}{298.15} \right) \right)$. The list of species that are modelled as distributed between liquid and gas phases, and their associated Henry constants and mass transfer coefficients are listed in Supplementary Table S2.

Modelling of medium pH. At the beginning of each timestep in the integration of the differential equation system (composed of Equations 3-6), the pH of the solution is determined. This is done by solving the charge balance of the system using the Brent method [33], while considering the proportion of each ionized species depending on the pH. The acid-base

equilibria that are considered and determined at each time step are listed in Supplementary Table S3, along with the associated pK values.

Model parameters and parameter calibration. The kinetic parameters used in the model are listed in Table S1, and are based on experimental estimates given in the literature. Henry constant and mass transfer coefficients (Table S2) are compiled from the literature or measured in this study (see below). The thermodynamic parameters are either calculated dynamically (as explained above) or adapted from the literature (Table 1). The only parameters of the model that are calibrated against experimental data are the $\Delta G^{i}_{\mathrm{min},j}$ of the different catabolic pathways. These parameters are calibrated using a recently introduced optimisation procedure [34]. This approach has been chosen because it has specifically been proposed in the context of the estimating microbial growth parameters and to circumvent the problem of parameter identifiability [35]. In brief, this approach calibrates multiple parameters (the $\Delta G^{i}_{\mathrm{min},j}$ of each pathway) against multiple observed variables (experimentally observed lactate, acetate, H_2(g) and CH_4(g) concentrations). With this optimisation procedure, the parameters are treated in a hierarchical fashion according to two properties; the extent (the number of variables affected upon changing a given parameter) and scale (the level of change in variables induced by changing a given parameter) of their effect. The parameter that produces the strongest effect amongst the least number of variables is selected first and the experimental time course data of the variables are weighted so that those variables that are most affected by the parameter have more weight in the calculation of the match between model prediction and experimental data during the optimisation procedure. The selected parameter is then optimized against the weighted experimental data on variables using the truncated Newton method (here we use the implementation available in the Python 3.4, package "scipy"). This method minimizes the weighted sum of squared distance between the model predictions and the experimental data on the variables. Once a parameter is optimized in this way, its value is fixed and removed from the list of the parameters to be optimized. The optimisation procedure then restarts with the remaining parameters until they have all been optimized and then repeated again for a different set of starting values. The whole process of optimisation is repeated until it yields no significant improvement anymore in terms of distance between the model predictions and the experimental data on variables.

Numerical simulations. The model is used to simulate the dynamics of the different populations as well as the key metabolites and system pH. Simulations were run to emulate the actual experiments in terms of run duration and initial starting conditions. The latter was assumed to be an equal biomass distribution among constituting species. To estimate this distribution, total biomass concentration in C-mol/L was approximated from the experimental OD (at 600nm) measurements at the start of the experiment (Supplementary Table S4) and using a previously calibrated relationship between OD and biomass using sulfate reducing bacteria (predominantly *Desulfovibrio vulgaris*) [36]; $\ln(DW) = 5.12 \cdot \mathrm{OD600} - 4.987$, where *DW* is the dry weight of the cells in g/L. We converted the resulting *DW* value to 1/C-mol by dividing it by the molecular weight of the generic molecule used to represent biomass ($C_1H_{1.8}O_{0.5}N_{0.2}$, [27]); 24.6 g.C/mol. The resulting biomass concentration was then evenly distributed between the existing populations to create the initial point for simulations.

Experimental estimation of k_La for H_2, CO_2 and CH_4. The k_La parameter for H_2, CO_2 and CH_4 was estimated based on experimental measurements using the same setup as in our experimental system. Anaerobic medium was prepared as previously described [37], containing 30mM Na-lactate and 7.5mM Na_2SO_4. Anaerobic culture tubes (Hungate tubes, Chemglass Life Sciences, Vine- land, NJ, USA) were prepared with 5mL medium and 0.1mL of 100 mM $Na_2S{\bullet}9H_2O$ in each tube, sealed in an anaerobic chamber station (MG500, Don Whitley) and autoclaved. The headspace gas pressure and composition of the tubes were measured using a micro gas-chromatograph (GC) (Agilent 490 micro-GC, Agilent Technologies) and recorded. A gas mixture of H_2, CO_2 and CH_4 was prepared by first flushing two 118mL serum bottles with 80% H_2 / 20% CO_2 gas mixture for 3 minutes at 0.5 L/min flow rate and balancing the final pressure to 1atm (101325 Pa). Then, 10mL of 90% CH_4 / 10% CO_2 gas mixture at 1atm was injected into each serum bottle using a gas tight glass syringe (Cadence Science, Inc., Italy). 2.0mL of the resulting gas mixture is injected into each of the prepared Hungate tubes using a gas tight glass syringe. The tubes were incubated under 37°C for more than 24 hours, in order to let the added gas to be equilibrated between the headspace and the aqueous phase. The tubes were then flushed with 100% N_2 for 2 minutes at a flow rate of 0.2 L/min and their headspace pressure brought to 1atm using sterile needle and filter. The tubes were then returned to the 37°C incubator, and brought out in replicates of 3 for temporal measurement of headspace gas composition at pre-determined intervals of 0, 1, 2, 4, 8 and 24 hours. The resulting temporal gas equilibration data is then used to estimate the k_La value for H_2, CO_2, and CH_4. Specifically, the k_La values were obtained by minimizing the sum of squared error between average observed measurements and the integration of the dynamics of gas transfer considered (see Equations 5 & 6).

Experimental implementation of monocultures and synthetic microbial communities. The three strains of *Dv*, *Mb* and *Mm* and anaerobic medium preparations were done as previously described [37]. In brief, the mono-cultures of *Dv*, *Mb* and *Mm* were cultivated in 5mL anaerobic media for 4, 21 and 7 days respectively to reach their late log phase. These monocultures were all grown at 37°C in the same anaerobic medium base (OSM1.0 media as described in [37]), but with different carbon and energy sources; 30mM Na-lactate and 10mM Na_2SO_4 for *Dv*, 100mM Na-acetate for *Mb* and 10mM Na-pyruvate and 68.4mM NaCl for *Mm*. For the last species, the headspace is also filled with 80%H_2 / 20%CO_2 gas mixture at a pressure of 2atm. To create synthetic communities of co- and tri-cultures, we first created stock cultures by taking 2mL aliquots of each monoculture using sterile needle syringe inside anaerobic chamber and inoculating these in the combinations of *Dv-Mb*, *Dv-Mm* and *Dv-Mb-Mm* into different serum bottles, which contained 50mL OSM1.0 medium with 30mM Na-lactate and 7.5mM Na_2SO_4. The inoculated serum bottles were placed in a 37°C incubator for 21 days. At the end of this period, 17.5mL cultures of different combinations from the incubated serum bottles were transferred into 500mL anaerobic Duran bottles containing 350mL of the above medium. The Duran bottles were linked to a Micro-GC (Agilent 490 micro-GC, Agilent Technologies) for the continuous monitoring of the methane production over two weeks. The active methanogenic communities in all combinations are confirmed in this way and the cultures were considered and used as the stock cultures for the following step. 5mL of the stock cultures from each combination were extracted inside anaerobic chamber, mixed separately with 5mL fresh anaerobic medium OSM1.0 with 30mM Na-lactate and 7.5mM Na_2SO_4 in Hungate tubes, and incubated at 37 °C for 7 days. These cultures formed the inocula for the following time-series experiment.

To measure temporal dynamics of co- and tri-cultures, as well as *Dv* monoculture, we designed a time-series experiment that involved starting a large number of replicate tubes and terminating a set of this large batch at different time points for gas and metabolite measurements. In total, 273 anaerobic Hungate tubes were prepared to collect data for 21 time points. Each tube contained 5mL OSM1.0 medium with 30mM Na-lactate and 7.5mM Na_2SO_4. According to the full reaction of sulfate reduction by *Dv* in Table 1, 7.5mM sulfate should allow *Dv* to convert 15mM lactate fully, while the conversion of the other 15mM lactate would rely on *Dv*'s other less thermodynamically favourable pathways. The tubes were numbered individually and separated into 21 batches. Each batch contains 13 tubes, of which 1 tube was used as blank control and 3 replicate tubes were used each for the 4 cultures: *Dv-Mb*, *Dv-Mm*, *Dv-Mb-Mm* and *Dv*, respectively. The tubes were inoculated with the respective cultures using the stock cultures described above, and following the tube and batch numbers. The initial optical density (OD) at 600nm and headspace pressure were recorded for each tube using a spectrophotometer (Spectronic 200E, Thermo Scientific) and a needle pressure gauge (ASHCROFT 310, USA). All tubes were incubated at 37°C. Over the following 21 days, 13 tubes of one batch were terminated on each single day to measure their OD at 600nm, pH (Mettler Toledo M300, Columbus, Ohio, USA), gas pressure (ASHCROFT 310, USA), gas composition using Micro-GC (Agilent 490 micro-GC, Agilent Technologies) and the lactate, acetate, pyruvate and sulfate concentrations using Ion Chromatography (Dionex ICS-5000$^+$ DP, Thermo Scientific) as described previously [37].

RESULTS AND DISCUSSION

To develop and calibrate a thermodynamic model of microbial growth and metabolite dynamics in a community context, we focus here on defined anaerobic synthetic communities. In particular, we use a recently developed experimental model system for studying syntrophic interactions among sulfate reducers and methanogens [37, 38], which make up a key part of anaerobic microbial communities found in AD reactors and freshwater and estuary sediments. The studied synthetic systems are composed of a representative sulfate reducer (*Desulfovibrio vulgaris*, *Dv*), and two different methanogens representing hydrogenotrophic (*Methanococcus maripaludis*, *Mm*) and hydrogeno/acetotrophic (*Methanosarcina barkeri*, *Mb*) methanogenesis pathways (see Materials and *Methods* and Figure 1). We have collected here data on metabolite dynamics over a 3-week period from *Dv* monocultures, *Dv-Mm* and *Dv-Mb* co-cultures, and *Dv-Mm-Mb* tri-cultures under specific media conditions (see *Materials and Methods*).

A comprehensive and generic thermodynamic model of community dynamics. To capture community and metabolite dynamics, we developed a comprehensive and expandable thermodynamic model that also accounts for metabolite phase exchanges and medium pH (see *Materials and Methods*). As is common for many microbes found in microbial communities, the species composing the studied synthetic communities can catalyse multiple, distinct metabolic pathways, sometimes starting from the same substrate. To account for these different metabolic activities of each species, we considered that each population can utilise any number of pathways at once, as previously described [30]. Each pathway consists of a catabolic (energy harvesting) reaction and an anabolic (biomass synthesis) reaction (Figure 1). The number of anabolic turnovers per catabolic turnover is then determined dynamically based on the energy flux provided by the catabolic reaction and on the cost of biomass production (see Equation 1). The latter is computed accounting for biomass synthesis cost and a constant "dissipation" cost per amount of biomass, based on recent estimations [28]. Therefore, this model implements a dynamic biomass yield based on energy considerations. By lumping all the catabolic energy that is not incorporated into biomass as a constant "dissipation" term, we implicitly assume

that maintenance (which is then part of dissipation) is constant. While more sophisticated dynamic representations of maintenance exist [39, 40], these approaches would add more complexity to the current model, which aims to assess how a simpler, more parsimonious thermodynamic modelling approach can capture experimental population dynamics.

The specific rate of the catabolic reaction is determined by the product of a kinetic factor (F_D), expressing enzyme kinetics, and a thermodynamic factor (F_T), expressing the limitations arising from thermodynamic constraints (see Figure 1 and Equation 2). F_T accounts for the energetic feasibility of growth-supporting pathway, as well as a minimal energy requirement (ΔG_{min}). The ΔG_{min} represents the concept that cells must invest some of the energy associated with each catabolic into a metabolic driving force to run that reaction, as well as into maintaining cell viability. It is assumed that such an energy investment is pathway specific and its value can be estimated from population dynamics data, as attempted here. The resulting model is parameterised for kinetic rates using available estimates for *Dv*, *Mm*, and *Mb* (see Table S1). After this parameterisation, the only unknown parameters in the system are the ΔG_{min}, which we have estimated here from the data, and some of the metabolite phase exchange constants, which we have determined experimentally. This model is developed in a generic manner allowing its expansion to include additional species and metabolic conversions. This makes it adaptable to other monocultures and natural or synthetic communities (see *Materials and Methods*).

One key feature of this generic thermodynamic model, differentiating it from previous similar models is that it implements dynamic metabolic stoichiometry through a variable yield term. The use of variable yield adjusted to close the energy balance of metabolism has indeed been advocated as a necessary feature to represent anaerobic metabolism dynamics [41, 42]. Moreover, determining the yield from physical quantities (energy gradients) reduces the amount of parameters to calibrate and thus improve the identifiability of the model's parameters [34]. Another feature of the model is the implementation of chemical speciation in order to get a more realistic representation of the pH dynamics and the chemical concentrations during the simulations. This point, while being a rather technical one, is important especially when a dissolved species involved in a metabolic pathway has also a counterpart in the gas phase (e.g. hydrogen). In such cases, the presented model accounts for the concentration of the dissolved species in the mass action ratio of a growth-supporting metabolic pathway when determining the Gibbs free energy of that pathway.

A thermodynamic inhibition model is required to correctly capture community metabolite dynamics. The F_T factor in the presented model introduces a mechanism for thermodynamic inhibition in the model, as done previously [17]. The same model without this factor could be considered as a purely 'forward reaction kinetics model' that considers catabolism as an irreversible process, limited only by substrate concentration [16, 22] _(see Figure 1 for illustration). We evaluate these two types of models in their ability to capture metabolite dynamics in our synthetic communities. As explained above, the model without the thermodynamic factor is nested in the presented model in the sense that it results from setting the F_T term to one in Equation 2. When we do so and use previously determined kinetic parameters (listed in Table S1), we can apply the resulting model without thermodynamic inhibition to the experimental data. We find that such a model is not able to explain the observed experimental results (Figure *2*). In particular, this model suggests full conversion of lactate in all culture conditions, while we do find significant lactate remaining in both *Dv* monoculture and *DvMb* co-culture. This qualitative mismatch between experiment and a non-thermodynamic inhibition model is directly a result of the structure of this model. Such a model

cannot account for the low energy of lactate fermentation in the absence of sulfate, and therefore incorrectly predicts that *Dv* can consume all of the lactate. Note that this result would not change if we allow fitting of kinetic parameters in the kinetic model, as there is no mechanism in the model to allow for 'shutting down' of lactate consumption. The thermodynamic model, instead, allows for such a mechanism through the F_T term in Equation 2, and as discussed in the next section, this feature allows it to better capture the experimental data.

Calibration of thermodynamic model allows prediction of minimal energy investments during growth with different metabolic pathways. The thermodynamic model allows better capturing of the metabolite dynamics, as shown in Figure 2. In this case, the model features additional ΔG_{min} parameters associated with the F_T term in Equation 2. As described above, this parameter captures the associated energy investment from each catabolic reaction into 'running' that reaction and into maintaining key cellular processes such as membrane potential. In order to determine this parameter for each of the possible metabolic pathways that can be used by *Dv*, *Mm* and *Mb*, we calibrated the model using an iterative fitting procedure described recently [34] (see *Materials and Methods*). The calibration process starts with an initial ΔG_{min} value of -40 kJ/mol, based on values from various sources for the Gibbs energy of formation of ATP [17, 43], and is applied using all possible combinations of the experimentally observed dynamics to result in the predicted ΔG_{min} values for each of the growth-supporting metabolic pathways (Table 2).

After a set of parameters was determined by the calibration procedure for each combination of observed variables, a parametric sweep was performed to determine whether the obtained values correspond to an optimum that minimizes the distance between simulation and observation. We assess this by plotting an error function (see *Materials and Methods*) for each calibrated parameter value (Figure 3 and S1-S4). The shape of the error function around the calibrated values of each parameters indicates that the ΔG_{min} of the lactate fermentation pathway has a clear optimum regarding the output variables considered (acetate and H_2 in gas phase), and lies between -30 and -15kJ/mol. The ΔG_{min} of the hydrogenic and acetoclastic methanogenesis pathways cannot be given an exact estimate but rather boundaries, between 0 and -20kJ/mol for hydrogenic methanogenesis and less negative than -40kJ/mol for hydrogenic methanogenesis (Figure 3A). The ΔG_{min} parameters for *Dv*'s sulfate respiration pathways could not be calibrated with the present experimental data, presumably because sulfate respiration occurs relatively quickly compared to the time-resolution of the available experimental data.

As far as we are aware, estimation of the ΔG_{min} parameter has only been attempted before in few studies [20, 30]. The minimal free energy for the three metabolic pathways of *Dv* (lactate fermentation and sulfate respiration with lactate or hydrogen) has been calibrated against experimental data only from monocultures grown in the presence of sulfate, and using a model similar to that presented here [30]. The experimental design in that study was different, using solely a monoculture (rather than monoculture and communities as we do here), sampling at shorter time intervals and using higher sulfate concentration than this study. Perhaps due to such differences, the estimated value from that study for lactate fermentation was -39.5 kJ/mol, relatively higher (i.e. more energy investment required as driving force and into maintenance) than found here. Possibly due to its use of higher sulfate concentration and shorter sampling intervals, that study was able to estimate the ΔG_{min} for both lactate and H_2 respiration on sulfate, as -44.66 kJ/mol. It should be noted that the model utilised by that study is different from the model used here, in that it uses gas partial pressure when calculating reaction free energies and has taken a static approach to model biomass yield. A theoretical study aimed at estimating

464 energetic parameters for several metabolic pathways, including methanogenesis, using existing
465 data [44], but, it used a notion of minimum energy threshold that requires assumptions about
466 the underlying metabolic reactions. The final minimum energy threshold is then expressed in
467 terms of ATP molecules produced per metabolic pathway turnover. The resulting predictions
468 from that study cannot be directly translated into a minimum energy threshold if we assume
469 that the Gibbs free energy carried by an ATP molecule varies dynamically with the state of the
470 cell's ATP pool, and therefore cannot be compared directly to the results presented here.
471
472 It is interesting to note that when a parameter sweep shows the existence of an optimal value
473 or range, these depend on the experimental variable and culture used for calibration (see Table
474 2, Figure 3B). There are two possible explanations for this observation. Firstly, there may be
475 metabolic pathways being catalysed by the populations in the different experimental batches
476 that are not represented by the model. If such pathways involve a specific metabolite, then
477 calibrations performed on that metabolite vs. some other metabolite might differ. Such an
478 explanation, while theoretically possible, does not fit with the fact that the presented model
479 accounts for all key pathways known to be catalysed by *Dv*, *Mm*, and *Mb*. The second possible
480 explanation is that the minimum energy threshold of a given metabolic pathway depends on
481 the experimental conditions. Indeed, the concept of a minimum energy threshold for growth
482 aims to conceptualise energy invested as metabolic driving force as well as cellular
483 maintenance. Both these energetic investments are expected to be a function of culture and
484 cellular conditions, including specific cellular details such as Mg^{+2} concentration [45]). The
485 minimum energy threshold of a growth-supporting pathway is then expected to be dynamic.
486 However, accurately predicting those dynamic variations would require to implement a
487 detailed model of the populations' metabolic networks and cellular states.
488
489 **CONCLUSIONS**
490 Here, we have developed and presented a generic thermodynamic model for capturing
491 population and metabolite dynamics in a microbial community. The model implements specific
492 features that have been proposed and advocated over the last two decades [22, 28, 33, 41] by
493 introducing factors based on first principles (thermodynamic limitation of reaction rate [47]).
494 As such, it overcomes the limitations of modelling approaches solely based on Michaelis-
495 Menten-type kinetics and empirically calibrated product inhibitions (such as with the ADM1
496 model [13]). We applied this model to capture the dynamics of synthetic communities
497 composed of a sulfate reducer and two methanogens. We also used the model to attempt an
498 estimation of the minimum energy thresholds of the different growth-supporting metabolic
499 pathways found in these organisms, sulfate respiration, lactate fermentation, and
500 hydrogenotrophic and acetoclastic methanogenesis. Our findings show that the presented
501 model, while simple, is indeed able to capture some of the thermodynamic limitations occurring
502 in the observed dynamics. Further, the use of the model on experimental data allows for the
503 prediction of the minimum energy requirements for sulfate fermentation and hydrogenotrophic
504 and acetoclastic methanogenesis.
505
506 Our calibration results also shed light on the limitations of the thermodynamic approach
507 employed. In particular, despite improvements over a non-thermodynamic model, the
508 presented model was not able to fully capture experimental metabolite and population
509 dynamics and its combination with experimental data did not allow to precisely determine the
510 minimal free energies for all modelled pathways. These limitations might be inherent in the
511 structure of the model or in the experimental design used here, or a combination of the two.
512 The latter can be addressed particularly by collecting more and higher resolution temporal data
513 from similar experimental systems. The former will probably require increasing the complexity

of the presented model. In particular, considering minimum energy thresholds as a constant feature of the system may be too simplistic and might instead require including elements of metabolic pathway dynamics within the bacterial growth models.

Thermodynamic constraints that we have endeavoured to predict here are one of the few phenomena that can be safely assumed to apply for all growth-supporting metabolic pathways. A sound basis for the description of this fundamental constraint applying to metabolic dynamics is thus necessary before attempting to assess and calibrate the extent of higher order phenomena such as genetic regulation or resource allocation [46, 47]. While further dedicated experiments and more complex models are necessary to improve the accuracy of dynamics predictions, the presented work provides a step towards this aim. The presented model expands previous efforts of minimal energy estimates from monocultures [30] and combines several recently proposed model features such as dynamic growth yield [22, 41] with additional features such as modelling of multiple pathways within individual species, phase exchange dynamics, and pH. As such, its further use and assessment will facilitate thermodynamic modelling of microbial community dynamics and estimation of energetic parameters, helping the development of more predictive microbial community dynamics models.

ACKNOWLEDGEMENTS

We thank Dr. Fred Farrell for his contributions to the software development of an earlier version of the presented model.

FUNDING

This work was funded by The University of Warwick and by the Biotechnological and Biological Sciences Research Council (BBSRC), with grant no. BB/K003240/2 (to O.S.S.) and no. BB/M017982/1 (to the Warwick Integrative Synthetic Biology Centre, WISB). M.J.W. acknowledges the support from the European Union's Horizon 2020 research and innovation programme under the Marie Skłodowska-Curie Grant Agreement No. 702408 (DRAMATIC).

AUTHOR'S CONTRIBUTIONS.

O.S.S. designed the overall study and contributed to model development. J.C contributed to design of experiments and performed them. M.W contributed to the design of the model and its initial implementation. H.D designed the model, implemented it and performed data fitting and model analyses. All authors contributed to the writing of the manuscript and have given approval to the final version.

TABLES

Organism	Catabolic pathway(s)	Anabolic pathway	Dissipated energy
Dv	$C_3H_5O_3^-$ + 2 H_2O → $C_2H_3O_2^-$ + 2 H_2(aq) + HCO_3^- + H^+ $\Delta G^{0'}$ = 27.58 kJ/mol	0.35 $C_3H_5O_3^-$ + 0.2 NH_4^+ + 0.1 H^+ → $C_1H_{1.8}O_{0.5}N_{0.2}$ + 0.05 $C_2H_5O_2^-$ + 0.4 H_2O $\Delta G^{0'}$ = 18.11 kJ/mol	ΔG_{dis} = -265.1 kJ/mol
	$C_3H_5O_3^-$ +0.5 SO_4^{-2} → $C_2H_5O_2^-$ + HCO_3^- + 0.5 H_2S(aq) $\Delta G^{0'}$ = -170.17 kJ/mol		ΔG_{dis} = -228.2 kJ/mol

	$H_2(aq) + 0.25\ SO_4^{-2} + 0.5\ H^+ \rightarrow 0.25\ H_2S(aq) + H_2O$ $\Delta G^{0'} = -56.33$ kJ/mol		$\Delta G_{dis} = -362.1$ kJ/mol
Mm	$0.25\ HCO_3^- + H_2(aq) + 0.25\ H^+ \rightarrow 0.25\ CH_4(aq) + 0.75\ H_2O$ $\Delta G^{0'} = -48.12$ kJ/mol	$HCO_3^- + 2.1\ H_2(aq) + 0.2\ NH_4^+ + 0.8\ H^+ \rightarrow C_1H_{1.8}O_{0.5}N_{0.2} + 2.5\ H_2O$ $\Delta G^{0'} = -64.73$ kJ/mol	$\Delta G_{dis} = -876.4$ kJ/mol
Mb	$0.25\ HCO_3^- + H_2(aq) + 0.25\ H^+ \rightarrow 0.25\ CH_4(aq) + 0.75\ H_2O$ $\Delta G^{0'} = -48.12$ kJ/mol $C_2H_3O_2^- + H_2O \rightarrow CH_4(aq) + HCO_3^-$ $\Delta G^{0'} = -14.65$ kJ/mol	$0.525\ C_2H_3O_2^- + 0.2\ NH_4^+ + 0.275\ H^+ \rightarrow C_1H_{1.8}O_{0.5}N_{0.2} + 0.05\ HCO_3^- + 0.4\ H_2O$ $\Delta G^{0'} = 28.63$ kJ/mol	$\Delta G_{dis} = -1059.8$ kJ/mol $\Delta G_{dis} = -1524.0$ kJ/mol

Table 1: Catabolic and anabolic reactions encoded by each species simulated in the presented model. Reaction Gibbs free energies are also shown, as calculated for pH=7, 1atm, and 310.15 K.

Culture	**Calibration variable**	**Lactate fermentation**	***Mm* Hydrogenotrophic methanogenesis**	***Mb* Hydrogenotrophic methanogenesis**	***Mb* Acetoclastic Methanogenesis**
Dv	$H_2(g)$	-30			
	Ac	-25			
DvMm	$H_2(g)$	<-30	>-25		
	Ac	-15			
	$CH_4(g)$		>-25		
DvMb	$H_2(g)$	-30			
	Ac	-25			
	$CH_4(g)$			>-23	>-32
DvMm Mb	$H_2(g)$	<-31	<-20	>-20	
	Ac	-15			
	$CH_4(g)$		<-30	>-25	>-25

Table 2: Calibrated ΔG_{min} values for the different growth-supporting metabolic pathways modelled in this study. All values are in kJ/mol. The different rows indicate the experimental data used for the calibration. Additional results from using combinations of experimental data are provided in the Supplementary Figures S1, S2, S3 and S4.

FIGURE LEGENDS

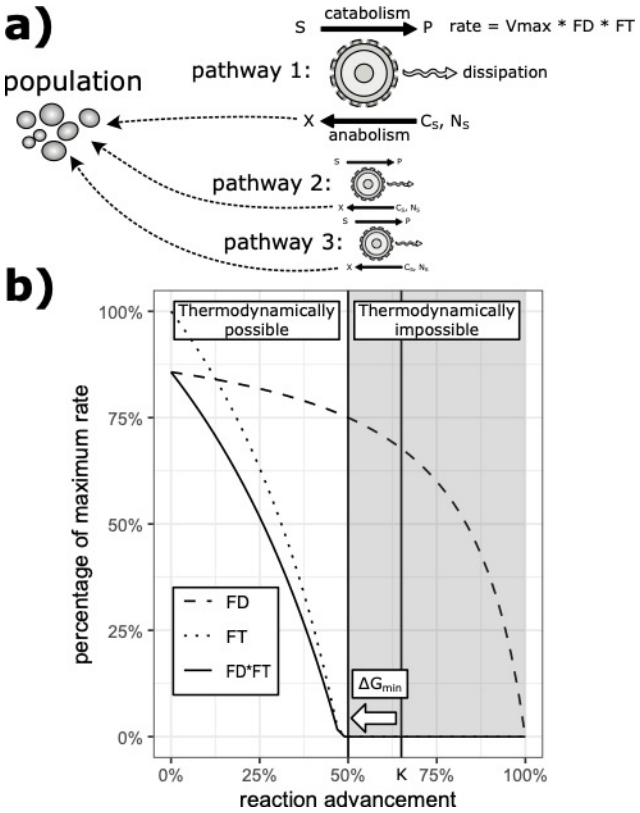

Figure 1. **(A)** Graphical summary of the presented model. Each microbial population is able to catalyse one to multiple different metabolic pathways. Each pathway consists in a catabolic reaction energetically coupled to an anabolic reaction. The rate of the catabolic reaction is given by a constant v_{max} multiplied by the F_D and F_T factors, representing enzyme kinetics and thermodynamics constraints respectively (see *Materials and Methods* and Equation 2). **(B)** Cartoon representation of the value of the F_D and F_T factors as a function of reaction advancement (this representation assumes a simple one-to-one substrate to product stoichiometry). Note that the greater the ΔG_{min} parameter is (as a negative number), the further left the point where *FD* becomes null moves.

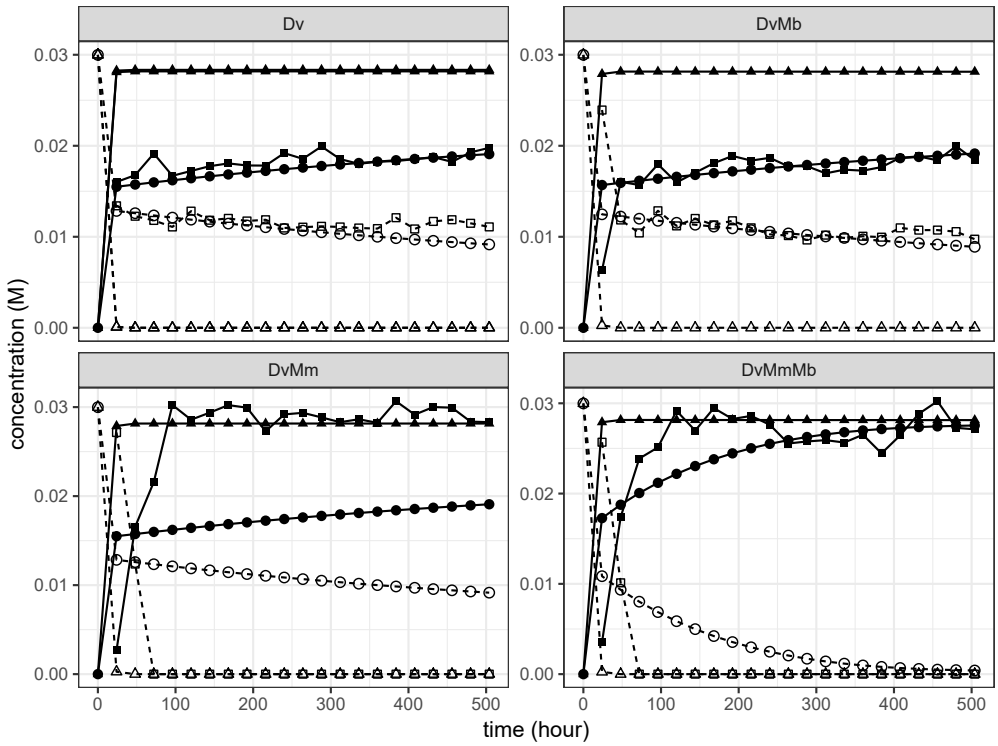

Figure 2. Concentration (mol/L) of acetate (solid line and filled shapes) and lactate (dashed line and empty shapes) over time (h) in the four different culture cases (*Dv*, *DvMm*, *DvMb*, *DvMmMb*) as measured in experiments (square) vs. simulated by the model (triangle or circle). Squares represent the median of the three experimental replicates, triangles represent simulations done without F_T factor (see Equation 2), circles represent simulations done with the F_T factor and using ΔG_{min} parameters obtained from calibration of the experimental data.

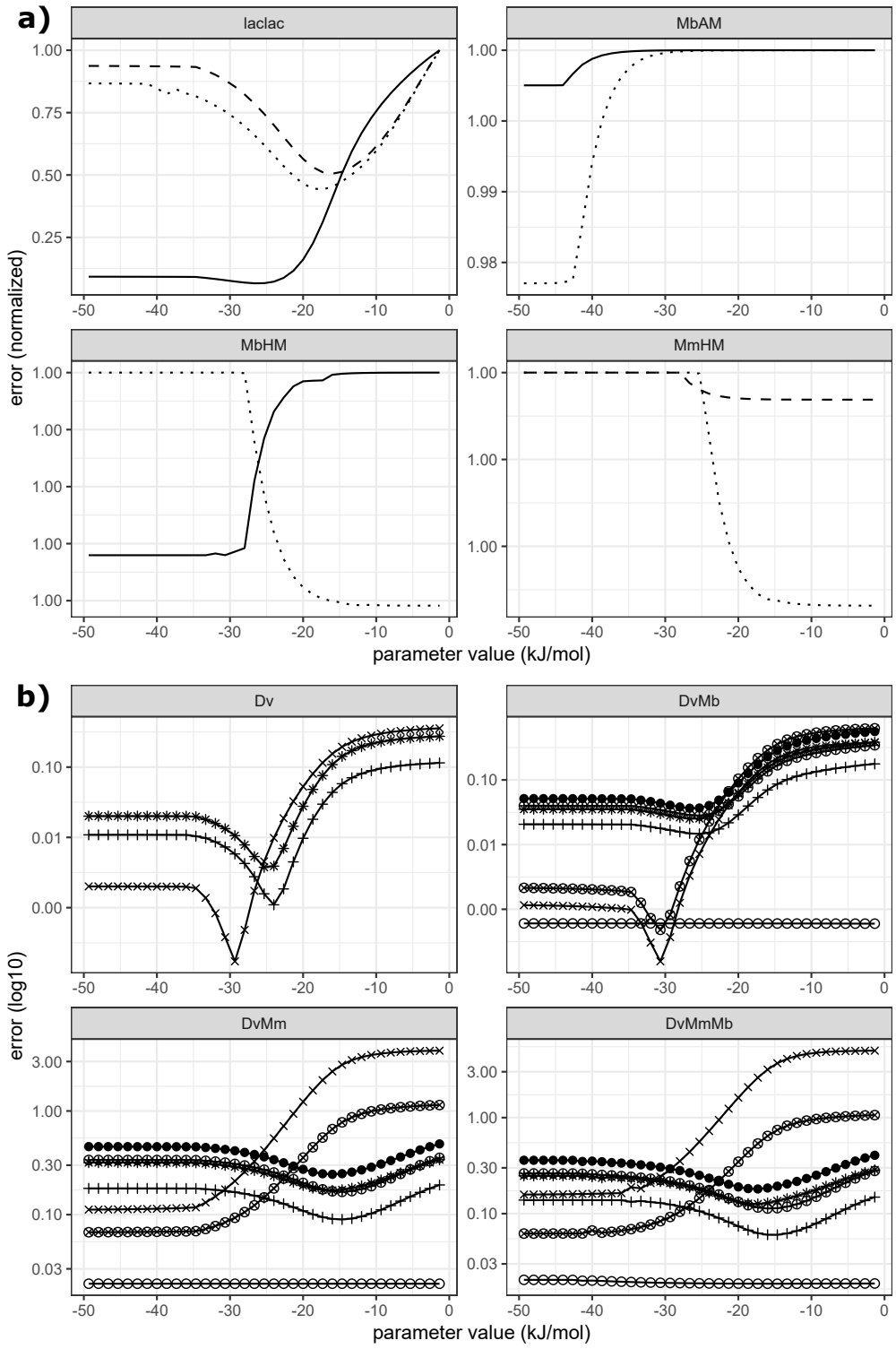

Figure 3. Sum of squared differences (error) between the experimentally observed variable(s) and the model prediction (y-axis) as a function of the value of the ΔG_{min} of various pathways (x-axis). **(A)** Normalised error between experimentally observed and predicted concentration of CH_4(g) and H_2(g) over time, depending on the values of ΔG_{min} for various pathways; lactate fermentation by *Dv* (laclac), acetoclastic methanogenesis by *Mb* (AM), hydrogenotrophic methanogenesis by *Mb* (HM) and hydrogenotrophic methanogenesis by *Mm* (HM). The error results shown are for the case using the experimentally observed H_2(g) and acetate concentrations as the comparison. Results for different cultures are indicated with the line

properties; solid line for *DvMb*, dashed line for *DvMm*, dotted line for *DvMmMb*. **(B)** Log of the error, as a function of the estimated value of the ΔG_{min} of the lactate fermentation pathway. Each tile corresponds to the results from a different culture case. The experimentally observed variables on which the error is computed are; acetate (plus), $H_2(g)$ (cross), $CH_4(g)$ (circle), acetate and $H_2(g)$- (plus and cross), $H_2(g)$ and $CH_4(g)$ (circle and plus), acetate and $CH_4(g)$ (circle and cross), and $H_2(g)$, acetate and $CH_4(g)$ (black filled circles).

REFERENCES

1. Falkowski PG, Fenchel T, Delong EF. The Microbial Engines That Drive Earth 's Biogeochemical Cycles. *Science* 2008; **320**: 1034–1039.
2. Nicholson JK, Holmes E, Kinross J, Burcelin R, Gibson G, Jia W, et al. Host-gut microbiota metabolic interactions. *Science* 2012; **336**: 1262–1267.
3. Bais HP, Weir TL, Perry LG, Gilroy S, Vivanco JM. the Role of Root Exudates in Rhizosphere Interactions With Plants and Other Organisms. *Annu Rev Plant Biol* 2006; **57**: 233–266.
4. Widder S, Allen RJ, Pfeiffer T, Curtis TP, Wiuf C, Sloan WT, et al. Challenges in microbial ecology: building predictive understanding of community function and dynamics. *ISME J* 2016; **10**: 2557–2568.
5. Sekirov I, Russell SL, Caetano M Antunes L, Finlay BB. Gut microbiota in health and disease. *Physiol Rev* 2010; **90**: 859–904.
6. Nelson MC, Morrison M, Yu Z. A meta-analysis of the microbial diversity observed in anaerobic digesters. *Bioresour Technol* 2011; **102**: 3730–3739.
7. Großkopf T, Soyer OS. Synthetic microbial communities. *Curr Opin Microbiol* 2014; **18**: 72–77.
8. Gonze D, Coyte KZ, Lahti L, Faust K. Microbial communities as dynamical systems. *Curr Opin Microbiol* 2018; **44**: 41–49.
9. Coyte KZ, Schluter J, Foster K. The ecology of the microbiome: Networks, competition, and stability. *Science* 2015; **350:** 663-666.
10. Momeni B, Xie L, Shou W. Lotka-Volterra pairwise modeling fails to capture diverse pairwise microbial interactions. *Elife* 2017.
11. Monod J. the growth of bacterial cultures. *Annu Rev Microbiol* 1949; **3**: 371–394.
12. Gompertz B. On the Nature of the Function Expressive of the Law of Human Mortality , and on a New Mode of Determining the Value of Life Contingencies. *Trans Br Mycol Soc* 1825; **115**: 513–583.
13. Batstone DJ, Keller J, Angelidaki I, Kalyuzhnyi S V, Pavlostathis SG, Rozzi A, et al. The IWA Anaerobic Digestion Model No 1 (ADM1). *Water Sci Technol* 2002; **45**: 65–73.
14. Wenying S. Acknowledging selection at sub-organismal levels resolves controversy on pro-cooperation mechanisms. *Elife* 2015; **4**.
15. Sari T, Wade MJ. Generalised approach to modelling a three-tiered microbial food-web. *Math Biosci* 2017; **291**: 21–37.
16. Hoh CY, Cord-Ruwisch R. A practical kinetic model that considers endproduct inhibition in anaerobic digestion processes by including the equilibrium constant. *Biotechnol Bioeng* 1996; **51**: 597–604.
17. Jin Q, Bethke CM. A New Rate Law Describing Microbial Respiration. *Appl Environ Microbiol* 2003; **69**: 2340–2348.
18. Schink B. Energetics of syntrophic cooperation in methanogenic degradation. *Microbiol Mol Biol Rev* 1997; **61**: 262–80.
19. von Stockar U, Maskow T, Liu J, Marison IW, Patiño R. Thermodynamics of microbial growth and metabolism: an analysis of the current situation. *J Biotechnol*

2006; **121**: 517–33.
20. Jin Q, Bethke CM. The thermodynamics and kinetics of microbial metabolism. *Am J Sci* 2007; **307**: 643–677.
21. Rodríguez J, Lema JM, Kleerebezem R. Energy-based models for environmental biotechnology. *Trends Biotechnol* 2008; **26**: 366–374.
22. Großkopf T, Soyer OS. Microbial diversity arising from thermodynamic constraints. *ISME J* 2016; 1–9.
23. González-Cabaleiro R, Ofiţeru ID, Lema JM, Rodríguez J. Microbial catabolic activities are naturally selected by metabolic energy harvest rate. *ISME J* 2015; **9**: 2630–2641.
24. Heijnen JJ, Van Loosdrecht MCM, Tijhuis L. A black box mathematical model to calculate auto- and heterotrophic biomass yields based on gibbs energy dissipation. *Biotechnol Bioeng* 1992; **40**: 1139–1154.
25. Button DK. Nutrient uptake by microorganisms according to kinetic parameters from theory as related to cytoarchitecture. *Microbiol Mol Biol Rev* 1998; **62**: 636–645.
26. Roels JA. Energetics and kinetics in biotechnology. 1983. Elsevier Biomedical Press.
27. Roels J a. Application of macroscopic principles to microbial metabolism. *Biotechnol Bioeng* 1980; **103**: 2–59; discussion 1.
28. Smeaton CM, Van Cappellen P. Gibbs Energy Dynamic Yield Method (GEDYM): Predicting microbial growth yields under energy-limiting conditions. *Geochim Cosmochim Acta* 2018; **241**: 1–16.
29. Jin Q, Bethke CM. Kinetics of Electron Transfer through the Respiratory Chain. *Biophys J* 2002; **83**: 1797–1808.
30. Noguera DR, Brusseau G a, Rittmann BE, Stahl D a. A Unified Model Describing the Role of Hydrogen in the Growth of Desulfovibrio vulgaris under Different Environmental Conditions. *Biotechnol Bioeng* 1998; **59**: 732–746.
31. Lewis WK, Whitman WG. Principle of gas absorption. *Ind Eng Chem* 1924; **16**: 1215–1220.
32. Sander R. Compilation of Henry's law constants (version 4.0) for water as solvent. *Atmos Chem Phys* 2015; **15**: 4399–4981.
33. Brent RP. Algorithms for Minimization without Derivatives. 1973. Englewood Cliffs, N.J., Prentice-Hall.
34. Ahmed W, Rodríguez J. Generalized parameter estimation and calibration for biokinetic models using correlation and single variable optimisations: Application to sulfate reduction modelling in anaerobic digestion. *Water Res* 2017; **122**: 407–418.
35. Rodriguez J, Premier GC, Guwy AJ, Dinsdale R, Kleerebezem R. Metabolic models to investigate energy limited anaerobic ecosystems. *Water Sci Technol* 2009; **60**: 1669–1675.
36. Bernardez LA, Lima LRPDA. Improved method for enumerating sulfate-reducing bacteria using optical density. *MethodsX* 2015; **2**: 249–255.
37. Chen J, Wade MJ, Dolfing J, Soyer OS. Increasing sulfate levels show a differential impact on synthetic communities comprising different methanogens and a sulfate reducer. *J R Soc Interface* 2019; **16**.
38. Hillesland KL, Stahl DA. Rapid evolution of stability and productivity at the origin of a microbial mutualism. *Proc Natl Acad Sci U S A* 2010; **107**: 2124–2129.
39. Van Bodegom P. Microbial maintenance: A critical review on its quantification. *Microb Ecol* 2007; **53**: 513–523.
40. Kempes CP, van Bodegom PM, Wolpert D, Libby E, Amend J, Hoehler T. Drivers of bacterial maintenance and minimal energy requirements. *Front Microbiol* 2017; **8**: 1–10.

690 41. Kleerebezem R, Stams AJM. Kinetics of syntrophic cultures: A theoretical treatise on
691 butyrate fermentation. *Biotechnol Bioeng* 2000; **67**: 529–543.
692 42. Rodríguez J, Lema JM, van Loosdrecht MCM, Kleerebezem R. Variable stoichiometry
693 with thermodynamic control in ADM1. *Water Sci Technol* 2006; **54**: 101–110.
694 43. Russell JB, Cook GM. Energetics of Bacterial Growth : Balance of Anabolic and
695 Catabolic Reactions. *Microbiol Rev* 1995; **59**: 48–62.
696 44. Jin Q, Bethke CM. Predicting the rate of microbial respiration in geochemical
697 environments. *Geochim Cosmochim Acta* 2005; **69**: 1133–1143.
698 45. Gout E, Rebeille F, Douce R, Bligny R. Interplay of Mg2+, ADP, and ATP in the
699 cytosol and mitochondria: Unravelling the role of Mg2+ in cell respiration. *Proc Natl*
700 *Acad Sci* 2014; **111**: E4560–E4567.
701 46. Reimers AM, Knoop H, Bockmayr A, Steuer R. Cellular trade-offs and optimal
702 resource allocation during cyanobacterial diurnal growth. *Proc Natl Acad Sci U S A*
703 2017; **114**: E6457–E6465.
704 47. Kafri M, Metzl-Raz E, Jonas F, Barkai N. Rethinking cell growth models. *FEMS Yeast*
705 *Res* 2016; **16**: 1–6.
706